Effect of cobalt content on non-isothermal crystallization kinetics of Fe-based amorphous alloys

Efecto del contenido de cobalto en la cinética de cristalización no-isotérmica de aleaciones amorfas base Fe

Carolina Parra-Velásquez [1]*, Darling Perea-Cabarcas [1], F. J Bolivar [1]

[1]Centro de Investigación, Innovación y Desarrollo de Materiales – CIDEMAT, Facultad de Ingeniería, Universidad de Antioquia. Calle 70 #52 – 21. C. P. 050010. Medellin, Colombia.

ABSTRACT: In the present study, FeSiBP and FeCoSiBP ribbons with a fully amorphous structure were made by melt spinning technique. A detailed analysis of the isochronal crystallization behavior is presented in this paper. The influence of cobalt on the crystallization kinetics of the alloys was studied under isochronal conditions using differential scanning calorimetry (DSC). Apparent and local activation energy values were determined by Kissinger, Ozawa and Kissinger-Akahira-Sunose (KAS) methods. The results indicate that appropriate amounts of cobalt can significantly enhance the thermal stability of Fe-based alloys, through an increase in nucleation activation energy from 538kJ/mol to 701kJ/mol, obtained by Kissinger method. Furthermore, with the method proposed by Matusita, it was possible to obtain global values for the Avrami exponent, noting that from a general perspective, Co changes the mechanism from diffusion controlled to interface controlled. This leads to the conclusion that the crystallization process is complex and takes place in more than one stage. Therefore, the determination of nucleation mechanisms and dimensional growth is difficult due to the inapplicability of the Johnson-Melh-Avrami (JMA) model. As such, a study under isothermal conditions is suggested, in order to achieve a full understanding of the mechanisms involved.

RESUMEN: En el presente estudio, se obtuvieron cintas de las aleaciones FeSiBP y FeCoSiBP con una estructura completamente amorfa mediante la técnica de "melt spinning"; en este artículo se presenta un análisis detallado del comportamiento de las aleaciones bajo cristalización isócrona La influencia del cobalto en la cinética de cristalización de las aleaciones se estudió bajo condiciones isócronas utilizando calorimetría diferencial de barrido (DSC por su sigla en inglés). Los valores de energía de activación local y aparente se determinaron mediante los métodos de Kissinger, Ozawa y Kissinger-Akahira-Sunose (KAS). Estos resultados indican que cantidades apropiadas de cobalto pueden mejorar significativamente la estabilidad térmica de las aleaciones base Fe a través de un aumento en la energía de activación de nucleación, pasando de 538 kJ/mol a 701kJ/mol, con el modelo de Kissinger. Además, con el método propuesto por Matusita, fue posible obtener valores globales para el exponente de Avrami, observando que, desde una perspectiva general, el Co cambia el mecanismo de crecimiento de controlado por difusión a uno controlado por interfaz, afirmando la complejidad del proceso de cristalización, que tiene lugar en más de una etapa. Por otro lado, la determinación de los mecanismos de nucleación y la dimensionalidad del crecimiento es difícil debido a la inaplicabilidad del modelo Johnson-Melh-Avrami (JMA), por lo que se sugiere un estudio en condiciones isotérmicas, con el fin de lograr un mayor entendimiento de los mecanismos implicados.

1. Introduction

Fe-based amorphous alloys are widely used in the electric and electronic industries due to their soft magnetic behavior, a consequence of their randomly atomic

* Corresponding author: Carolina Parra Velásquez

E-mail: carolina.parrav@udea.edu.co

structure. This behavior makes them suitable for a wide number of applications, such as sensors, inductors and transformer cores, where high saturation magnetization and permeability values, as well as the lowest possible coercivity and losses, are required [1–3]. When used as cores, these materials are forced in some cases to bear high temperatures, and, as is well-known, most material properties change under these conditions [4]. Knowledge of the crystallization behavior of metallic glasses, considering thermodynamic and kinetic parameters, helps elucidate the nucleation and growth mechanisms, allowing the thermal stability of the material to be established [5, 6].

In addition to providing information about the thermal limits of the material that allows high temperature degradation in work conditions to be avoided [4], knowing the crystallization behavior and kinetic parameters also permits accurate temperatures and times for annealing treatments to be determined. This is relevant when the goal is to modify physical, mechanical or magnetic properties through the precipitation of specific phases achieved by partial or total devitrification, treatments widely used with this type of materials, depending on the final application [7].

Crystallization kinetics in amorphous alloys are usually determined either by isothermal or isochronal treatments. In the former, the material is heated in the supercooled liquid region and maintained at this temperature until the crystallization process is completed. In the latter, the material is heated continuously at different rates to temperatures above that of crystallization [8, 9]. In the present work, a crystallization kinetics study was performed under isochronal or non-isothermal conditions, as most Fe-based alloys are treated in this way [3, 10–13]. Global activation energies (E_a), both nucleation (associated to inset crystallization temperature–T_{x1}) and growth (associated to peak temperature–T_p) [14], are determined by Kissinger (Equation 1) [15] and Ozawa (Equation 2) [11] methods. Meanwhile, local values, ie. activation energy as a function of crystallized volume fraction χ, $E_a(\chi)$, are given by the isoconvertional method proposed by Kissinger-Akahira-Sunose (KAS) (Equation 3) [16, 17]. From DSC curves and partial area technique, the crystallized volume fraction χ can be calculated as $\chi = S/S_0$ where S corresponds to the area at any temperature between the onset and the end of the exothermic event, and S_0 to the total area under the peak [18].

E_a values are related to the slope of the $1/T$ vs. $Ln(\beta/T^2)$ plot for Kissinger and KAS methods, and the slope of $1/T$ vs. $Ln(\beta)$ plot for Ozawa's method.

$$Ln\frac{\beta}{T^2} = -\left(\frac{E_a}{RT}\right) + C \tag{1}$$

$$Ln(\beta) = -1.056\frac{E_a}{RT} + C \tag{2}$$

$$Ln\left(\frac{\beta}{T_\chi{}^2}\right) = -\frac{E_\chi}{RT_\chi} + C \tag{3}$$

Where:

β: Heating rate

T: Selected characteristic temperature (Tx1 and Tp1 in this case)

T_χ: Temperature at a specified χ, this being the crystallized volume fraction

R: Gas constant $= 8.314$ J/mol·K

E_a: Activation energy

In addition, the Avrami exponent (n) reflects the nucleation and growth mechanisms presented in the alloy as it heats and crystallizes, and gives information about process dimensionality. The model proposed by Johnson, Melh and Avrami is used to determine "n" in alloys treated under isothermal conditions [16, 19]; however, under some assumptions, it can be used in non-isothermally treated alloys [20]. The normalized function $z(\chi) = \varphi T^2$ model [21] is used to determine the applicability of the JMA due to the non-linearity of the JMA plots ($Ln[-Ln(1-\chi)]$ vs $Ln(1/T)$). This function is evaluated with respect to χ, and enables the applicability of the model to be confirmed if the maximum is 0.632 ± 0.02 [22]. On the other hand, it is not possible to use the JMA model to describe the crystallization kinetics of the alloy, so another approach is necessary. The method proposed by Matusita *et al.* [23] is the approach suggested in the present work. This method proposes the determination of the Avrami exponent with the slope of the $Ln\beta$ vs $Ln[-Ln(1-\chi)]$ plot, according to Equation 4.

$$Ln[-Ln(1-\chi)] = -nLn\beta - 1.052\frac{mE}{RT} + C \tag{4}$$

Where n and m are the numeric factors depending on the nucleation process and growing morphology. $n = m + 1$ when the amorphous alloy does not have pre-existing nuclei, and $n = m$ when there is a sufficient number of nuclei in the alloy [12, 23].

Crystallization kinetics in metallic glasses is a widely-covered topic in the context of Fe-based alloys, both amorphous and nanocrystalline. Nevertheless, the system proposed in the present research has not been previously reported. Most FeCo-based alloys achieve their nanocrystalline structure through either rare and expensive glass forming elements such as Nb, Zr or Mo, or small amounts of Cu [13, 24]. The aim of this research was to obtain good properties in an amorphous alloy, with

a view to reducing costs and avoiding post-production treatments. In the present study, it was possible to obtain amorphous alloys of the $(Fe_{1-x}Co_x)_{77}Si_8B_{10}P_5$ system in ribbon shape, using melt spinning technique. A kinetic analysis under isochronal conditions was carried out in order to determine the effect of cobalt on the thermal stability of the Fe-based system. Kinetic parameters analysis was based on the first exothermic reaction because it is at this stage, which is the most intense and is associated with the α-Fe soft magnetic phase, where the properties of these kinds of alloys are most affected.

2. Experimental methodology

2.1 Materials

Master alloy ingots with the composition of each selected system: $Fe_{77}Si_8B_{10}P_5$, $(Fe_{0.8}Co_{0.2})_{77}Si_8B_{10}P_5$ and $(Fe_{0.6}Co_{0.4})_{77}Si_8B_{10}P_5$, were prepared by induction melting in a vacuum chamber under argon atmosphere, starting with stoichiometric mixtures of powders of Fe (Aldrich Chemistry - $\geq$99% - CAS 7439-89-6), Co (American Elements - 99.95% - CAS 7440-48-4), Si (Aldrich Chemistry - 99% - CAS 7440-21-3), FeB (American Elements - 99% - CAS 12006-84-7) and Fe_2P (Alfa Chemistry - 99% - CAS 1310-43-6). The alloy compositions represent nominal percentages. Rapidly solidified ribbons were prepared from the master alloy ingots by melt spinning in air [25] at atmospheric pressure conditions, using argon as the ejection gas, with a copper wheel of 250 mm diameter and quartz crucibles with 1mm nozzle. The wheel speed was between 35 and 40 m/s, the gap between the wheel and the crucible was 400 μm, an ejection pressure of 200 mbar was employed, and the ejection temperatures were between 1480 and 1500 K. These parameters were determined by the researchers based on previous experiments.

2.2 Methods

Structural characterization of the as-spun ribbons was performed by X-ray diffraction (XRD), using a PANalytical Empyream diffraction system with Co-Kα (λ=1.789010 Å) radiation, with 2θ between 30 and 110º. Complementary structural analysis was performed by transmission electron microscopy (TEM) using a FEI Tecnai G2-F20 super twin microscope. The characteristic temperatures of the material were evaluated by differential scanning calorimetry (DSC) at a heating rate of 20 K/min, in order to determine kinetic parameters. Treatments at 5, 10 and 30 K/min were also executed. All thermal analyses and heat treatments were performed using a TA Instruments SDT Q600 simultaneous TGA/DSC under a constant argon flow.

3. Results and discussion

3.1 Structural characterization and thermal analysis

With the parameters mentioned above, ribbons with 2 mm width and 15-25 μm thickness were obtained. Both wheel and air surfaces were smooth and clean and, more importantly, an amorphous structure was achieved. This can be seen in the XRD patterns shown in Figure 1, in which only a broad diffuse peak centered at $2\theta = 52^o$, with no sharp diffraction peaks corresponding to crystalline phases, is observed. TEM images of the base alloy are presented in Figure 2. Here, three structures are presented: as-cast (Figure 2a), where a fully amorphous structure can be seen without any evidence of atom clusters; after heat treatment at 833K, where the presence of some crystals embedded in the remaining amorphous matrix is evident (Figure 2c); and after the crystallization process is completed, where a fully crystalized structure with grains between 50 and 100nm can be seen.
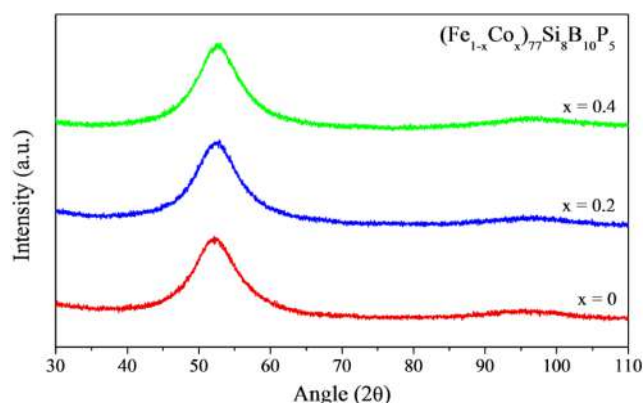

Figure 1 XRD patterns of the $(Fe_{1-x}Co_x)_{77}Si_8B_{10}P_5$ system with x = 0, 0.2 and 0.4 metallic glass ribbons

DSC curves obtained for the system at the heating rates mentioned are presented in Figure 3. As can be seen, the base alloy only exhibits one exothermic event, while Co-modified alloys display two. The presence of one exothermic event indicates that the alloy crystallizes in one stage; hence, all the forming phases precipitate simultaneously. Meanwhile, the presence of two exothermic events implies that the crystalline phases precipitate in two stages, suggesting that cobalt enhances the thermal stability of alloys.
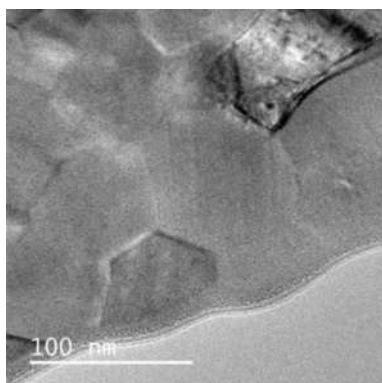
In order to make an appropriate analysis of the crystallization process of the Co-modified alloys, it is necessary to isolate the first peak, which is associated with the soft magnetic phase α-Fe. The separation was done by the Gaussian two-peak fitting method, and the isolated peaks are shown in Figure 4. From this figure, the
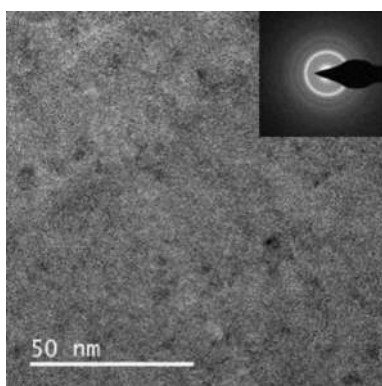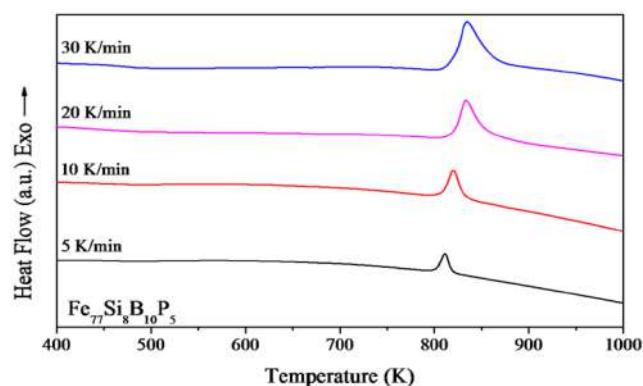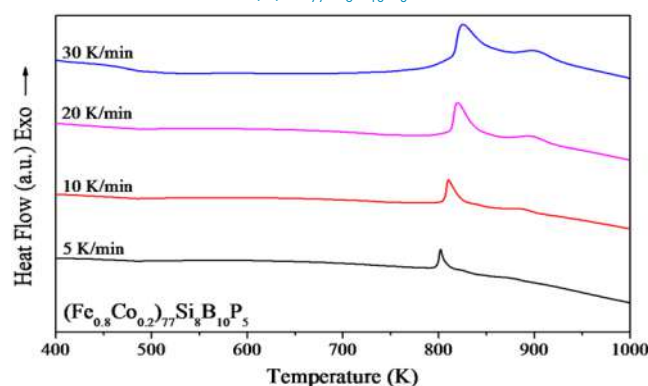
(a) As-cast
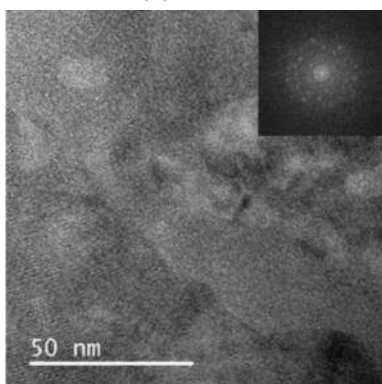
(b) After heat treatment at 833K
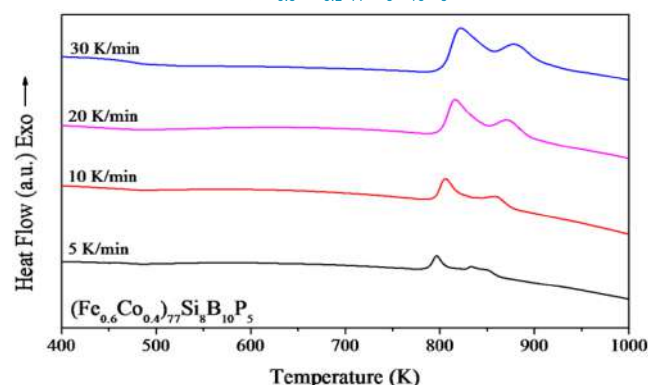

(c) After heat treatment at 923K

Figure 2 TEM images of base alloy ($Fe_{77}Si_8B_{10}P_5$)

(a) $Fe_{77}Si_8B_{10}P_5$

(b) $(Fe_{0.8}Co_{0.2})_{77}Si_8B_{10}P_5$

(c) $(Fe_{0.6}Co_{0.4})_{77}Si_8B_{10}P_5$

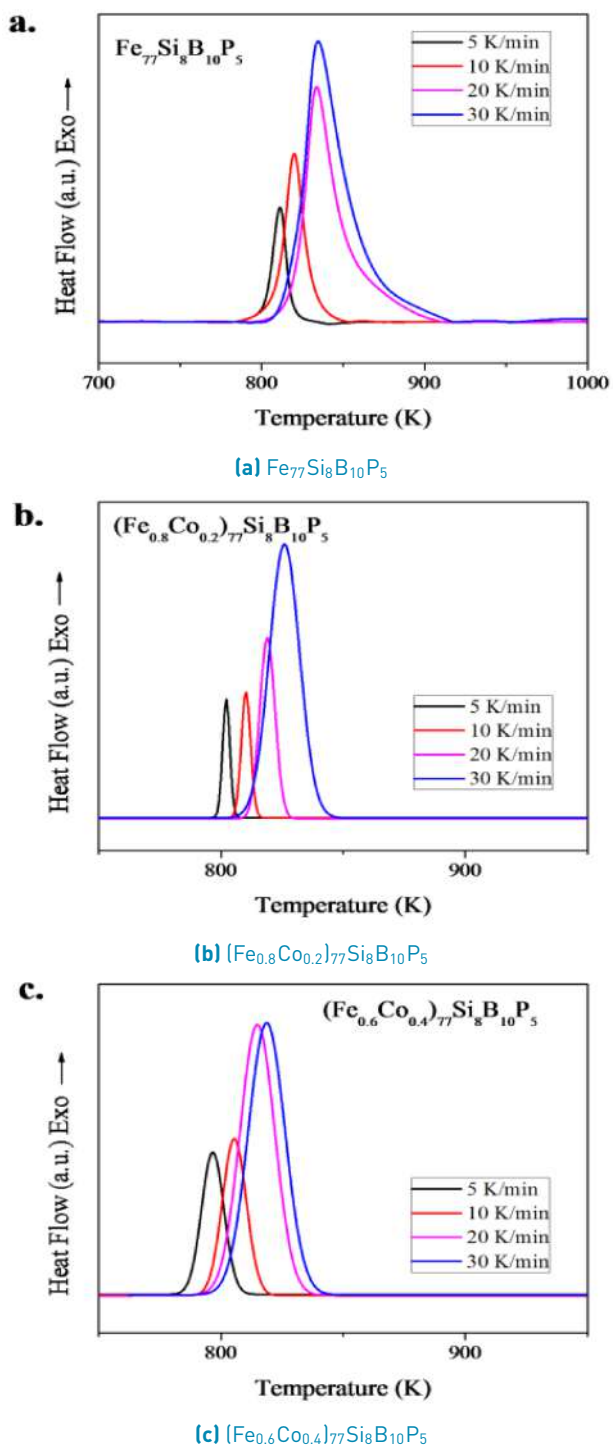**Figure 3** DSC curves obtained at different heating rates

thermodynamic effect, generating a shift towards the right as the heating rate increases and leading to a consequent increase in onset temperatures and heat flow, can be evidenced.

3.2 Activation energy

Apparent activation energy values are determined by Kissinger and Ozawa methods for both the nucleation and growth processes. Table 1 shows activation energy values obtained from the methods mentioned above (Equations 1–2). From these results, it can be concluded

that the values obtained for both methods are similar, and the small variations can be attributed to the different approximations used by each method. From Table 1 it is clear that the nucleation process is severely affected by Co presence, considering that E_a values are much higher for Co-modified alloys than for the Co-free alloy. However, the changes with cobalt addition in E_a values for growth are less evident.

From the nucleation values, it can be inferred that cobalt plays an important role in atomic mobility, since with low content $(x = 0.2)$, the energy barrier that

47

(a) $Fe_{77}Si_8B_{10}P_5$

(b) $(Fe_{0.8}Co_{0.2})_{77}Si_8B_{10}P_5$

(c) $(Fe_{0.6}Co_{0.4})_{77}Si_8B_{10}P_5$

Figure 4 Isolated peaks for each alloy system at different heating rates

Table 1 Apparent activation energy values of nucleation and growth

	Ea nucleation (kJ/mol)		Ea growth (kJ/mol)	
X	**Kissinger**	**Ozawa**	**Kissinger**	**Ozawa**
0	538.007	524.194	373.883	367.868
0.2	789.148	763.494	407.028	399.919
0.4	701.917	679.904	417.046	409.351

higher cobalt concentrations $(x = 0.4)$, a reduction in thermal stability with respect to the previous Co content is evidenced. Moreover, growth activation energy monotonically increases with Co content, despite that fact that in all cases nucleation values are higher than growth values. This suggests that in the Fe-based amorphous alloys developed in the present work, the nucleation process is more difficult than the growth process, and the energy required to initiate crystallization is superior to that required for the rest of the process. The higher values of activation energy for Co-modified alloys than for the base alloy are consistent with the interpretation provided by the DSC results regarding the effect of cobalt on the thermal stability of alloys, and can be associated with the presence of two exothermic events.

The lack of definition of the second exothermic event in the alloy with $x = 0.2$ could represent an obstacle to atomic mobility, increasing the energy barrier and delaying the beginning of the nucleation process, resulting in the values being higher. Similarly, due to the better definition of the second peak in the $x = 0.4$ alloy, a superior separation of the phase precipitation at each stage and, therefore, a slight decrease in activation energy values, is achieved.

Apparent activation energy represents the average energy of the whole crystallization process. However, owing to the complex nature of this process in this type of alloy, the mechanisms can differ from one stage to another, which makes a local analysis of kinetic parameters necessary. With the crystallized fraction and KAS method, local activation energy values are obtained. In Figure 5, the curves for each system are presented. The strong dependence of activation energy on crystallized fraction can be noted based on the curves, verifying that crystallization is a multiple-stage process. These results are consistent with the values obtained for apparent activation energy, where the energy barrier to start the crystallization process (nucleation) is higher than the barrier for the subsequent growth; reinforcing the assertion that the process progresses gradually, from a high difficulty level (high $E(\chi)$ values) to an easier one (lower $E(\chi)$ values).

Crystallized volume fraction evolution as a function

must be overcome to start the nucleation process is significantly higher than for the base alloy. This indicates that the precipitation tendency of the crystalline phases in this type of alloy decreases and, as a consequence, thermal stability is greater, which is also associated with a higher glass forming ability [14]. However, with
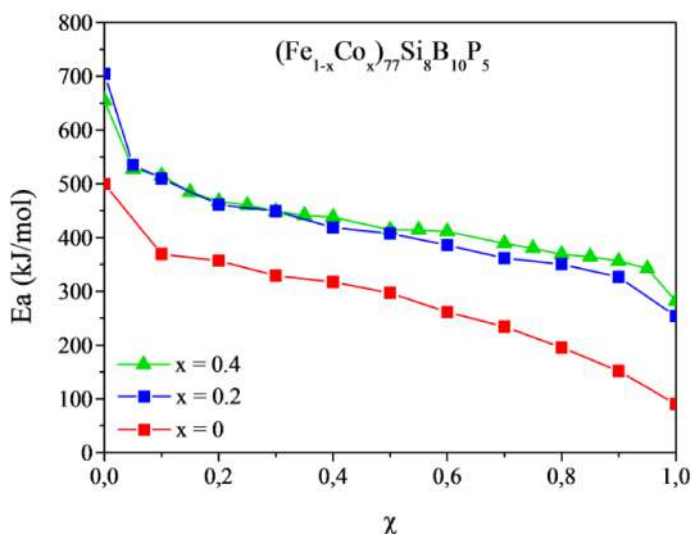
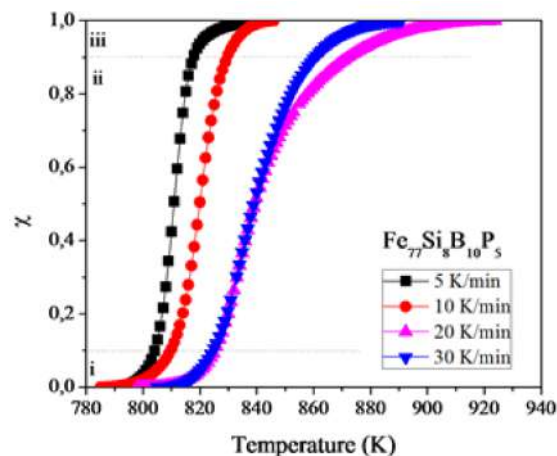**Figure 5** Local activation energy curves for the $Fe_{77}Si_8B_{10}P_5$, $(Fe_{0.8}Co_{0.2})_{77}Si_8B_{10}P_5$ and $(Fe_{0.6}Co_{0.4})_{77}Si_8B_{10}P_5$ alloys

(a) $Fe_{77}Si_8B_{10}P_5$

(b) $(Fe_{0.8}Co_{0.2})_{77}Si_8B_{10}P_5$

(c) $(Fe_{0.6}Co_{0.4})_{77}Si_8B_{10}P_5$

Figure 6 Crystallized volume fractions curves as a function of temperature for the alloys
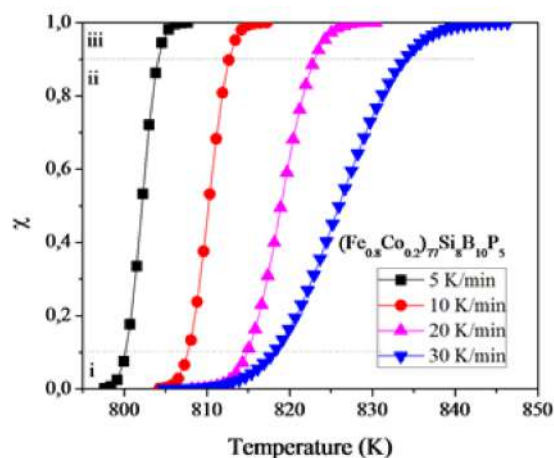
of temperature at different heating rates is presented for the three alloys in Figure 6. All the curves have sigmoidal shapes, suggesting that the crystallization takes place in three stages marked i, ii and iii in each graph, which correspond respectively to the first, second, and third stage. As all three alloys present the same behavior, the following explanation of each stage is valid for all the compositions studied.

In the first stage, corresponding to the section marked "i" in the graphs, the crystallized fraction (χ) is between 0 and 0.1. This stage corresponds to the beginning of the crystallization process. The reaction rate is low, indicating that the crystallization occurs slowly. At this stage, nucleation is the dominant process, and is characterized by nuclei precipitation at different points of the amorphous matrix (nucleation). This stage can be associated with the "$\chi < 0.1$" section of Figure 5, suggesting that the low reaction rate is due to the high energy needed to start the crystallization process, but that once it is reached, the crystallization process proceeds faster. This is shown in the second stage of the sigmoidal curves (marked "ii" in the graphs), covering values of χ from 0.1 to 0.9, where the crystallized fraction drastically rises due to the growth of the nuclei and its surface area.
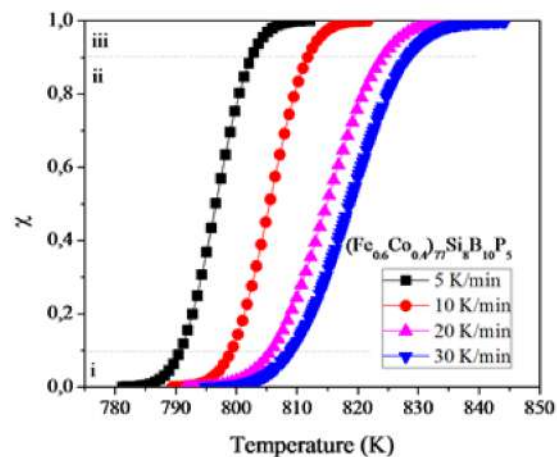
Finally, in the third stage (marked "iii" in the graphs), with χ values from 0.9 to 1, the crystallization rate decreases due to the impingement of the crystals and a reduction in the surface area between the crystallized phase and the amorphous matrix, and the crystallization process is gradually completed.

3.3 Avrami exponent

For the Avrami exponent determination, $Ln\left[-Ln\left(1-\chi\right)\right]$ vs. $Ln1/T$ plots are developed and presented in Figure

7. At certain areas of the curves, linear behavior can be observed. Study of this kinetic parameter under JMA model can be considered, as a first approximation. Nevertheless, the activation energy results and non-linear areas of the curves lead to the conclusion that the nucleation and growth mechanisms fluctuate during the process. With this in mind, the applicability of the JMA model is validated with $z\left(\chi\right)$ normalized function.

Table 2 presents the maximum values for the normalized function $z\left(\chi\right)$. It is clear that all the values differ from the characteristic value of this function in the JMA model $(0.632 \pm 0.02$ [22]), indicating that it cannot be used to describe the crystallization behavior of the exothermic event and that it is therefore necessary to use a different approach. In this case, the Matusita *et al.* method, described above, is used.

Table 2 Maximum values for the normalized function $z\left(\chi\right)$ for each alloy at different heating rates

Heating rate (β)	χ at max $z\left(\chi\right)$ max		
	C42 (x=0)	C47 (x=0.2)	C56 (x=0.4)
5	0.506953	0.532347	0.501565
10	0.504612	0.531761	0.574225
20	0.332405	0.590552	0.606290
30	0.368805	0.499106	0.647296

According to Matusita *et al.*, in order to evaluate the kinetic parameters n and m, three temperatures are taken within each exothermic event, and Avrami exponent values are obtained from the slope of the $\mathrm{Ln}\left[-\mathrm{Ln}\left(1-\chi\right)\right]$ vs $\mathrm{Ln}\beta$ plots. Table 3 presents the n and m values obtained.

Based on the values obtained for n and m, and assuming complete absence of pre-existing nuclei, it can be concluded that the nucleation mechanisms of the alloys are as follows: For the base alloy, one dimension diffusion controlled growth with decreasing nucleation rate; for the low Co-content alloy, interface controlled growth with increasing nucleation rate; and for the high Co-content alloy, two-dimension interface controlled growth with nucleation rate close to zero [23]. However, from Table 3, it is obvious that the values obtained for n at different temperatures differ considerably from each other, suggesting the existence of different mechanisms throughout the whole crystallization process, and demonstrating the need for a local analysis to further elucidate the crystallization kinetics. An isothermal treatment, or the combined methods proposed by Málek and Šesták-Berggren, suggested in [26], could be helpful in studying the crystallization kinetics of this type of Fe-based alloys.
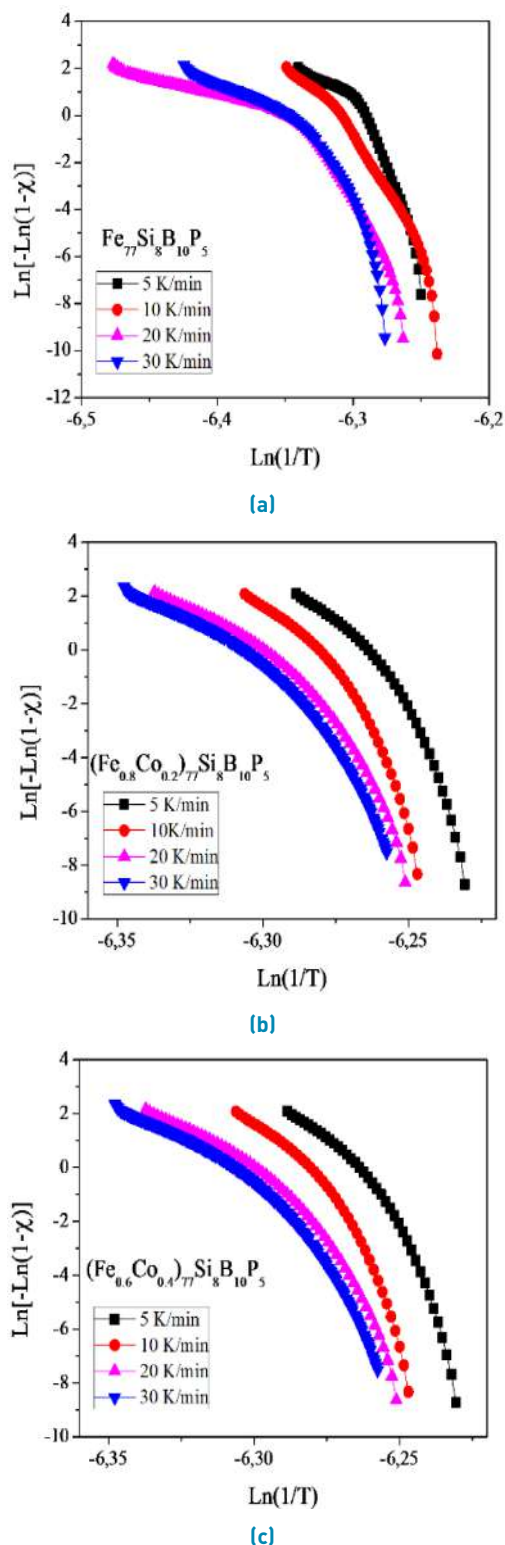
Figure 7 Avrami exponent determination for (a) $Fe_{77}Si_8B_{10}P_5$, (b) $(Fe_{0.8}Co_{0.2})_{77}Si_8B_{10}P_5$ (c) $(Fe_{0.6}Co_{0.4})_{77}Si_8B_{10}P_5$ alloys

4. Conclusions

From the research described, it can be concluded that:

Table 3 n and m values obtained with Matusita *et al.* method

	T_1	T_2	T_3	n	m
C42 (x=0)	3.075860	2.591390	1.602440	2.423	1.423
C47 (x=0.2)	4.999290	4.875220	4.719950	4.865	3.865
C56 (x=0.4)	3.365540	2.815530	2.027280	2.736	1.736

- Cobalt promotes an increase in nucleation activation energy, making it necessary to overcome a high energy barrier in order to start the crystallization process, evidence of improved thermal stability, and that once the energy barrier is overcome, the crystallization process evolves quickly and easily.

- With the method proposed by Matusita, it was possible to obtain global values for the Avrami exponent, noting that Co changes the mechanism from diffusion controlled to interface controlled, and demonstrating that the crystallization process is complex and takes place in more than one stage.

- The determination of nucleation mechanisms and growth dimensionality is difficult due to the inapplicability of the JMA model.

- The isochronal treatment and the isokinetic method do not fulfill the requirements to explain these mechanisms.

5. Acknowledgements

References

[1] Metglas(R) Inc. (2016) Amorphous metal distribution transformers. [Online]. Available: https://bit.ly/2WZMSN3

[2] V. Franco and O. Gutfleisch, "Magnetic materials for energy applications," *J. Miner. Met. Mater. Soc.*, vol. 64, no. 7, June 29 2012. [Online]. Available: https://doi.org/10.1007/s11837-012-0348-7

[3] L. J. Wang, J. Q. Li, and H. J. Wang, "Application of nanocrystalline magnetic materials in electromechanical devices," *Mater. Sci. Forum*, vol. 694, July 27 2011. [Online]. Available: https://doi.org/10.4028/www.scientific.net/MSF.694.341

[4] A. H. Taghvaei and J. Eckert, "A comparative study on the isochronal and isothermal crystallization kinetics of $Co_{46.45}Fe_{25.55}Ta_8B_{20}$ soft magnetic metallic glass with high thermal stability," *J. Alloys Compd.*, vol. 675, August 2016. [Online]. Available: https://doi.org/10.1016/j.jallcom.2016.03.053

[5] S. D. Kaloshkin and I. A. Tomilin, "The crystallization kinetics of amorphous alloys," *Thermochim. Acta*, vol. 280-281, July 1996. [Online]. Available: https://doi.org/10.1016/0040-6031(96)02926-7

[6] J. Malek, "Kinetic analysis of crystallization processes in amorphous materials," *Thermochim. Acta*, vol. 355, no. 1-2, July 2000. [Online]. Available: https://doi.org/10.1016/S0040-6031(00)00449-4

[7] B. Vishwanadh, D. Srivastava, R. Balasubramaniam, and G. K. Dey, "A study on synthesis, crystallization, and magnetic behavior of nanocrystalline Fe-Based metallic glasses," *Metall. Mater. Trans. A*, vol. 39, no. 7, pp. 1560–1572, Jul. 2008.

[8] Y. Ma, B. Rheingans, F. Liu, and E. J. Mittemeijer, "Isochronal crystallization kinetics of $Fe_{40}Ni_{40}B_{20}$ amorphous alloy," *J. Mater. Sci.*, vol. 48, no. 16, pp. 5596–5606, Aug. 2013.

[9] Q. P. Cao and *et al.*, "Isochronal crystallization kinetics of $Cu_{60}Zr_{20}Ti_{20}$ bulk metallic glass," *J. Non. Cryst. Solids*, vol. 357, no. 3, February 2011. [Online]. Available: https://doi.org/10.1016/j.jnoncrysol.2010.10.030

[10] T. Paul, A. Loganathan, A. Agarwal, and S. P. Harimkar, "Kinetics of isochronal crystallization in a Fe-based amorphous alloy," *J. Alloys Compd.*, vol. 753, July 2018. [Online]. Available: https://doi.org/10.1016/j.jallcom.2018.04.133

[11] T. Ozawa, "Kinetic analysis of derivative curves in thermal analysis," *J. Therm. Anal.*, vol. 2, no. 3, pp. 301–324, Sep. 1970.

[12] J. Vázquez, C. Wagner, P. Villares, and R. Jiménez, "A theoretical method for determining the crystallized fraction and kinetic parameters by DSC, using non-isothermal techniques," *Acta Mater.*, vol. 44, no. 12, December 1996. [Online]. Available: https://doi.org/10.1016/S1359-6454(96)00127-9

[13] T. Gheiratmand and *et al.*, "Effect of annealing on soft magnetic behavior of nanostructured $(Fe_{0.5}Co_{0.5})73.5Si13.5B9Nb3Cu1$ ribbons," *J. Alloys Compd.*, vol. 582, January 2014. [Online]. Available: https://doi.org/10.1016/j.jallcom.2013.08.038

[14] H. Wei and *et al.*, "Crystallization kinetics of $(Ni_{0.75}Fe_{0.25})78Si10B12$ amorphous alloy," *J. Non. Cryst. Solids*, vol. 354, no. 17, April 2008. [Online]. Available: https://doi.org/10.1016/j.jnoncrysol.2007.10.009

[15] H. E. Kissinger, "Reaction kinetics in differential thermal analysis," *Anal. Chem.*, vol. 29, no. 11, November 01 1957. [Online]. Available: https://doi.org/10.1021/ac60131a045

[16] Z. F. Yao, J. C. Qiao, C. Zhang, J. M. Pelletier, and Y. Yao, "Non-isothermal crystallization transformation kinetics analysis and isothermal crystallization kinetics in super-cooled liquid region (SLR) of $(Ce_{0.72}Cu_{0.28})_{90} - {}_xAl_{10}Fe_x$ (x = 0, 5 or 10) bulk metallic glasses," *J. Non. Cryst. Solids*, vol. 415, May 2015. [Online]. Available: https://doi.org/10.1016/j.jnoncrysol.2015.02.017

[17] P. Rezaei, A. Seifoddini, and S. Hasani, "Thermal stability and crystallization process in a Fe-based bulk amorphous alloy: The kinetic analysis," *J. Non. Cryst. Solids*, vol. 471, September 2017. [Online]. Available: https://doi.org/10.1016/j.jnoncrysol.2017.05.044

[18] A. Pratap and A. T. Patel, "Crystallization kinetics of metallic glasses," in *Advances in Crystallization Processes*, Y. Mastai, Ed. Shanghai, China: InTech, 2012, pp. 107–126.

[19] J. C. Qiao and J. M. Pelletier, "Crystallization kinetics in $Cu_{46}Zr_{45}Al_7Y_2$ bulk metallic glass by differential scanning calorimetry (DSC)," *J. Non. Cryst. Solids*, vol. 357, no. 14, July 2011. [Online]. Available: https://doi.org/10.1016/j.jnoncrysol.2010.12.071

[20] D. W. Henderson, "Thermal analysis of non-isothermal crystallization kinetics in glass forming liquids," *J. Non. Cryst. Solids*, vol. 30, no. 3, January 1979. [Online]. Available: https://doi.org/10.1016/0022-3093(79)90169-8

[21] Y. Zhi, D. Shu, W. Xiang, and L. Pei, "Applicability

of johnson-mehl-avrami model to crystallization kinetics of $Zr_{60}Al_{15}Ni_{25}$ bulk amorphous alloy," *Trans. Nonferrous Met. Soc. China*, vol. 18, no. 1, February 2008. [Online]. Available: https://doi.org/10.1016/S1003-6326(08)60025-4

[22] A. H. Moharram, A. M. Abdel, and F. S. Shokr, "Crystallization kinetics of the $Se_{80}Te_{15}Sb_5$ glass," *Chalcogenide Lett.*, vol. 13, no. 9, pp. 435–442, Sep. 2016.

[23] K. Matusita, T. Komatsu, and R. Yokota, "Kinetics of non-isothermal crystallization process and activation energy for crystal growth in amorphous materials," *J. Mater. Sci.*, vol. 19, no. 1, May 1984. [Online]. Available: https://doi.org/10.1007/BF02403137

[24] R. Li and *et al.*, "Crystallization and magnetic properties of $[(Fe,Co)_{0.75}Si_{0.05}B_{0.20}]_{94}Nb_6$ metallic glasses," *J. Phys. D. Appl. Phys.*, vol. 42, no. 8, April 01 2009. [Online]. Available: https://doi.org/10.1088/0022-3727/42/8/085006

[25] C. Suryanarayana and A. Inoue, "Synthesis of bulk metallic glasses," in *Bulk Metallic Glasses*, C. Suryanarayana and A. Inoue, Ed. New York, USA: CRC Press, 2011, pp. 145–186.

[26] Z. Jamili, M. Haddad, J. Vahdati, and Y. Ke, "Thermal behavior and non-isothermal crystallization kinetics of $(Ti_{41}Zr_{25}Be_{28}Fe_6)_{93}Cu_7$ bulk metallic glass," *J. Non. Cryst. Solids*, vol. 447, September 01 2016. [Online]. Available: https://doi.org/10.1016/j.jnoncrysol.2016.05.043